Effect of Fiber Structure on Yield Stress during Enzymatic Conversion of Cellulose

Emilio J. Tozzi and Michael J. McCarthy
Dept. of Food Science and Technology, University of California, Davis, Davis, CA 95616

David M. Lavenson, Maria Cardona, and Robert L. Powell
Dept. of Chemical Engineering and Materials Science, University of California, Davis, Davis, CA 95616

Nardrapee Karuna and Tina Jeoh
Dept. of Biological and Agricultural Engineering, University of California, Davis, Davis, CA 95616

DOI 10.1002/aic.14374
Published online February 6, 2014 in Wiley Online Library (wileyonlinelibrary.com)

Enzymatic hydrolysis of cellulose for conversion to chemicals or fuels presents engineering challenges due to the large changes in suspension viscosity and yield stress that occur. A flow reactor with an in-line rheometer was used to investigate the role of changes in fiber structure on rheology. The evolution of the suspension yield stress was compared to amount of soluble sugars released and changes in fiber length and width. A model was constructed that links the yield stress, conversion, and fiber shape. These results provide insights into the relationship between fiber structure and transport properties during the early stages of hydrolysis of cellulosic biomass. © 2014 American Institute of Chemical Engineers *AIChE J*, 60: 1582–1590, 2014

Keywords: rheology, cellulose hydrolysis, fiber structure, magnetic resonance imaging, on-line measurement

Introduction

The hydrolysis of cellulosic biomass into sugars is a key step in bioprocesses that use microorganisms to produce chemicals or fuels. Although such processes are attractive as sustainable alternatives to fossil fuels, it is challenging to make the bio-based processes competitive with oil, coal, or natural gas.[1] One of the factors that increase process costs is the number of steps involved, which includes pretreatment, saccharification, fermentation, and separation. Many initial studies of cellulose hydrolysis have been performed under relatively dilute conditions (i.e., under 10% (w/w) concentration of total insoluble solids); these conditions are very favorable for laboratory-scale operations because low viscosities facilitate mixing and the large amounts of water used (low fiber concentration) keeps the inhibitor concentrations low. The dilute regime, however, is detrimental to process economics, since it requires high volumes of water which must be treated, heated, and distilled at great energy expense. Larger equipment sizes required for dilute processing also contribute to high capital costs. For these reasons, recent research has focused on operating at high solids loadings.[2–9]

The fibrous nature of cellulosic materials causes cellulosic slurries to be very viscous at high solids loadings, which makes mixing difficult. This causes a process bottleneck, since the quality of mixing between enzyme and substrate is critical to achieve sufficiently rapid reaction rates.[9–11] The insoluble solids concentrations at which mixing limitations can occur depend on the fiber characteristics. Long fibers, such as those derived from wood, can entangle and resist flow at concentrations below 10% (w/w) solids,[12] whereas for shorter fibers such as those from pretreated corn stover and other more intensively pretreated substrates, elevated viscosities are found at loadings of 20% (w/w) solids and greater.[13,14]

In a study by Zhang et al. performed at high solids loadings, a conventional kinetic model used by the authors was adequate to predict reaction rates at the later stages of saccharification of a cellulosic sludge, but the model failed to predict hydrolysis kinetics during the initial stages that occur at high solids concentrations. The authors hypothesized that the discrepancy is due to mass transfer limitations.[15] A deeper understanding of the phenomena that take place during the initial stages of hydrolysis is, therefore, of great importance for developing accurate models and efficient processes for more economic and sustainable production of cellulose-based fuels and chemicals.

A better understanding of the physical changes the biomass may be undergoing can be obtained from studying its rheological changes during hydrolysis. The crowding number, N, defined as $N=2/3\phi a_r^2$, is a function of the fiber aspect ratio (a_r) and volume fraction (ϕ), and has been used to characterize concentration regimes in the context of fiber–fiber interactions.[16,17] The quadratic dependence on a_r implies that fiber aspect ratio has a strong influence on fiber–fiber interactions. Small crowding numbers ($N \ll 1$) correspond to concentration regimes where fibers do not

M. J. McCarthy is also affliated with Dept. of Biological and Agricultural Engineering, University of California, Davis, Davis, CA 95616.

Correspondence concerning this article should be addressed to E.J. Tozzi at etozzi@aspectimaging.com.

interact. As the crowding number increases, large changes in rheology may occur over a narrow range of N. In the range of $N > 3$, it is considered that a fiber network forms and the properties are dominated by strong interactions among fibers.[17] Characterizing biomass suspensions in terms of crowding numbers can, thus, give additional insight regarding rheological changes and behavior during hydrolysis.

Among the parameters needed to design large-scale mixers and pumps is the suspension rheological behavior. Rheological monitoring using conventional off-line rotational rheometers presents various challenges. One of them arises from the so-called "gap size effect." Accurate measurements using rotational rheometers require particles to be much smaller than the smallest characteristic dimension of the rheometer. Since biomass particles of industrial interest can have sizes of the order of millimeters or larger, the relative size condition is not satisfied in rheometers with gaps of similar dimensions. Other challenges include particle settling, slippage on the surfaces in contact with the suspension, or expulsion of liquid in double plate rheometers.[13] Some of these challenges can be alleviated using large gap sizes, roughened plates, and attachments to avoid expulsion of the sample. Another class of challenges arises from the long times required to perform an off-line measurement. From the moment that a sample is taken to the moment that a rheogram is obtained, several minutes, hours, or days can pass and the sample may have suffered changes during handling and storage. The small sizes of the samples used in conventional rheometers also require means of ensuring that the sample is representative of the total reaction. All of these challenges indicate the underlying need for a fast, on-line rheological monitoring technique for biomass hydrolysis.

The main goal of this work is to characterize the rapid rheological changes that occur during early enzymatic hydrolysis using experiments and models. Cellulosic fibers were hydrolyzed in a recycle reactor equipped with instrumentation for in-line, noninvasive monitoring of slurry rheology. The rheological measurement is performed using magnetic resonance imaging (MRI), with which rheograms can be obtained in a matter of seconds.[18] Changes in slurry rheology over time are compared to conversion rates and changes in fiber shape, providing insights on the prevalent mechanisms that govern this important initial phase of hydrolysis. A simple model is presented that connects rheology and kinetics.

Materials and Methods

Experimental setup

Figure 1 is a schematic of the flow system used for these studies. The suspensions were loaded into a stainless steel mixing tank with a conical bottom and 10 L total volume (Toledo Spinning Co., Toledo, OH) connected to a Moyno positive displacement pump (Moyno, Springfield, OH) that circulates the suspension at a rate of 9 L/min. The suspension flowed through a heat exchanger coil submerged in a 23-L thermostatic bath (PolyScience 9610, PolyScience, Niles, IL) to maintain the hydrolysis temperature at $50 \pm 1°C$; temperature was also monitored with an inline type K thermocouple placed immediately after the imaging section. The pipes were insulated to reduce heat losses to the environment and keep the entire system under isothermal conditions. The heat exchanger coil was a helix with five

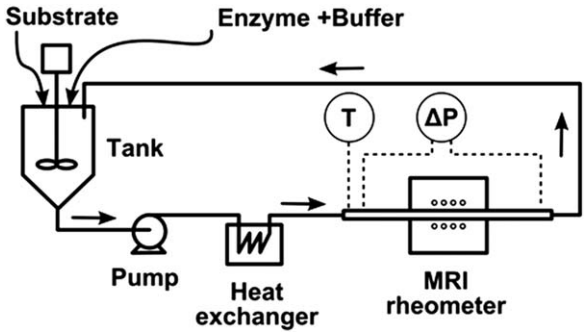

Figure 1. Experimental MRI flow loop setup for continuous hydrolysis.

turns, 121 mm in radius, with pitch of 48.2 mm, made of copper tubing with 17.3-mm internal diameter, and 0.89-mm thick walls. The suspension flowed through an acrylic tube 2.08-m long with an internal diameter of 18.5 mm. The acrylic tube was located in the imaging section of a MRI system described below. Finally, flexible piping returned the suspension to the mixing tank. Pressure drops were measured between taps at the opposing ends of the acrylic tube using a differential pressure transducer with a range of 0–25 kPa (PX770, Omega Engineering, Stamford, CT).

Magnetic resonance based rheometer

The MRI system is an Aspect Imaging MR100 1 Tesla MRI spectrometer (Aspect Imaging, Shoham, Israel), with 30 G/cm peak gradient strength. The radio frequency coil for flow imaging is a solenoid with three turns, encasing a cylindrical volume 38 mm in diameter and 36 mm long. Velocity profiles are obtained using a velocity encoded Pulsed Gradient Spin Echo sequence. The yield stress of the slurry is calculated from measured velocity images and pressure drops.[18] The procedure consists of the following steps: (a) an MRI velocity image is obtained[19]; (b) a velocity profile as a function of radial position, $v = v(r)$, is constructed from the image; and (c) a set of shear rates $\dot{\gamma}(r)$ is obtained by differentiation of the velocity profile. The corresponding shear stresses are computed as a function of the radius as $\tau(r) = -(\Delta P r)/(2L_P)$ where $\Delta P/L_P$ is the pressure drop per unit length (L_P is the length of the pipe). After completing step (c) one obtains a table with three columns. The first column of the table contains radii. The second column are shear rates corresponding to the radii of column one. The third column are shear stresses corresponding to the radii of column one. Columns two and three now constitute a rheogram, that is, a table of shear rates and shear stresses. (d) The yield stress $\tau_{y,}$ is computed from the rheogram.[18]

Previous researchers have performed rheological fits to various models, including Herschel-Bulkley, Bingham plastic, and power law models, all of which tend to fit the data well in the narrow range of shear rates typically measured. The yield stress can alternatively be determined by measuring the plug radius from the velocity profile.[18,20] In this work, we report the yield stress computed using the Bingham plastic equation based on the two data points with the lowest shear rates. The values obtained using other methods are similar.[21]

It must be noted that the methodology to obtain rheograms and rheological parameters from combined measurements of velocity profiles and pressure drops has been used

extensively by many researchers. Additional references on the methodology as applied to optical, ultrasound, and MRI velocimetric methods can be found in Tozzi et al.[22]

Cellulosic fibers

Two types of fibers with different average fiber aspect ratios were used. They are two grades (C100 and 200EZ) of commercial cellulosic fibers (Solka-Floc, International Fiber Corporation, Tonawanda, NY). The moisture content of the fibers was measured using a Mettler-Toledo model HR83 Halogen Moisture Analyzer (Mettler-Toledo International, Columbus, OH).

The chemical composition of the fibers, as shown in Table 1, was determined as per NREL laboratory analytical procedures.[24,25] Ash content was obtained as the mass of inorganic residue remaining after ignition at 575 ± 15°C for 24 h. The sugars were analyzed using the sugar measurement method by high performance liquid chromatography (HPLC) detailed below.

Enzymatic hydrolysis

Hydrolysis was performed at 50°C in 50 mM sodium citrate buffer at pH 4.76.[26] The enzyme used was Accelerase 1500 (Batch number 1601096506, DuPont Danisco, Copenhagen, Denmark) at a loading of 15 filter paper units/g-cellulose for each sample. Initial solids loadings were 7.7% (w/w) for the C100 and 16% (w/w) for the 200EZ; these solids loadings were chosen such that both suspensions were pumpable and had approximately the same initial crowding numbers. The total mass was 6.8 kg for the C100 (long fibers), and 8.05 kg for 200EZ (short fibers). Included in the total mass are fibers, buffer salts, water, and enzyme. The enzyme was added in one portion after all the biomass was added. The enzyme addition time is designated as "time zero." Samples of 25 mL were extracted at the time points of 0, 10, 20, 30, 40, 60, 90, 120, and 150 min after addition of the enzyme. Samples in sealed containers were then quenched in boiling water for 5 min to inactivate the enzymes.[26] Samples were stored in a freezer at −15°C prior to measurement of sugars and fiber geometry. A few drops of the quenched slurry were placed on a Petri dish and imaged to observe the morphology of the fibers using an optical microscope with digital camera (Nexcope CM500 series, Ample Scientific, Norcross, GA).

Fiber length and width

Fiber sizes were measured with an L&W FiberTester (Lorentzen and Wettre, Kista, Sweden). Values reported are length-weighted average lengths and length-weighted average widths. Length-weighted averaging is recommended to characterize properties that are dominated by longer fibers.[27] The number of fibers used in the averaging ranged from 7876 to 12254. The instrument used has been reported to have a repeatability of 0.011 mm for measuring length weighted length of pulps.[28]

Sugar content measurement by HPLC

Solubilized sugar concentrations in the hydrolyzates were analyzed by HPLC (Shimadzu Scientific Instruments, Columbia, MD). Separation was carried out on an Aminex HPX-87P column with deashing and Carbo-P guard cartridges (BioRad, Hercules, CA) and sugar concentrations were measured by refractive index. The flow rate was 0.6 mL/min at 80°C using nanopure water as the mobile phase. Calibration was performed with standard solutions of D-glucose, L-arabinose, D-xylose, D-mannose, D-galactose, and D-cellobiose. Conversions were calculated based on the measured concentrations of glucose, cellobiose, and xylose using equations from Roche et al.[11] The mass fraction of insoluble solids (FIS) and its volume fraction were calculated assuming negligible entrained liquid.[11]

Table 1. Properties of Fibers Used

Property	C100 (long)	200EZ (short)
Moisture content (%)	7.91	9.26
Mean length (length weighted) (mm)	0.444	0.331
Mean width (length weighted) (μm)	34.7	36.8
Ash (%)	0.10 ± 0.06	0.20 ± 0.010
Acid insoluble residue (%)	2.6 ± 0.4	3.0 ± 0.4
Glucan (%)	71.5 ± 1.2	67.7 ± 8.7
Xylan (%)	7.1 ± 0.10	7.3 ± 0.8
Mannan (%)	5.1 ± 0.10	4.3 ± 0.5
k_x	78.6 ± 1.2	75 ± 9

The compositional analysis was performed according to Hames et al.[23] and Sluiter et al.[24,25] Error bars are the standard error of triplicates. Acid insoluble residue includes the insoluble ash.

Measures of fiber concentration

We used three measures of fiber concentration:

1. Solids loading, defined as the mass fraction of insoluble solids, FIS.
2. Volume fraction of fibers, ϕ, defined as the volume of fibers per unit volume of suspension.[11]
3. Crowding number, N, defined as

$$N = 2/3\phi\, a_r^2, \tag{1}$$

where $a_r = L/W$ is the aspect ratio, or fiber length L divided by fiber width W.[17]

Results and Discussion

The suspensions of long and short fibers (C100 and 200EZ, respectively) were hydrolyzed in two separate experiments using the system shown in Figure 1. The parameters measured in the experiments are summarized in Table 2 for the long and short fibers. Examples of the images obtained using the magnetic resonance flow imaging method at different hydrolysis times are shown in Figure 2, which also has micrographs to illustrate the initial and final morphology of the cellulosic fibers. The MRI were processed as explained in the Materials and Methods Section to obtain on-line rheological measurements. In Figure 3, we show curves of viscosity as a function of shear rate and time for the two types of fibers obtained via MRI. The large variation of viscosity within a narrow range of shear rates indicates shear thinning behavior. The shear thinning behavior observed is consistent with previous reports of the rheology of fibrous biomass.[13,14,29–35] The shift of the apparent viscosity curves toward lower viscosity as the enzymatic hydrolysis progresses was previously reported for other cellulosic substrates, such as pretreated corn stover,[29] pretreated barley straw,[31] and pretreated poplar.[34] We will focus on the yield stress as a critical suspension property.[14]

In Figure 4, the yield stress as a function of time is shown. The large changes observed during the initial few

Table 2. Measured Parameters for Hydrolysis of Solka Floc C100 and 200EZ Fibers

Fiber Type	Time (min)	Cellobiose (g/L)	Glucose (g/L)	Xylose (g/L)	Conversion (%)	Fraction of Insoluble Solids (FIS)	Volume Fraction	Yield Stress (Pa)	L (mm)	W (μm)	Crowding Number (N)
C100 (long)	0	0.00	0.14	0.42	0.0	0.0768	0.0525	18.4	0.444	34.7	5.73
	10	0.00	5.81	0.60	8.1	0.0719	0.0491	3.43	N/A	N/A	N/A
	20	0.00	9.08	0.61	12.6	0.0692	0.0473	1.20	0.347	34.0	3.28
	30	0.00	10.91	0.81	15.5	0.0675	0.0461	1.07	0.339	34.1	3.04
	40	0.00	10.90	0.97	15.7	0.0673	0.0460	0.53	0.348	33.9	3.23
	60	0.00	11.69	0.95	16.7	0.0667	0.0456	0.51	0.319	34.2	2.64
	90	0.29	15.53	1.36	23.1	0.0629	0.0430	0.47	0.284	34.0	2.00
	120	0.00	13.09	1.53	19.5	0.0650	0.0445	0.43	0.281	34.1	2.01
	150	0.00	19.41	1.68	28.6	0.0595	0.0407	0.48	0.272	34.1	1.73
200EZ (short)	0	0.00	0.11	0.08	0.0	0.1600	0.1125	25.7	0.331	36.8	6.07
	5	0.00	10.99	2.03	8.1	0.1502	0.1057	4.88	0.296	34.8	5.10
	10	0.00	16.52	1.49	11.3	0.1464	0.1030	2.98	0.270	35.5	3.97
	20	0.00	17.79	1.28	12.0	0.1456	0.1025	2.43	0.265	35.0	3.92
	30	0.00	22.11	3.00	15.9	0.1409	0.0992	1.91	0.286	34.8	4.47
	40	0.00	24.40	3.20	17.5	0.1390	0.0979	1.24	0.256	34.7	3.55
	60	0.00	28.05	3.45	20.0	0.1359	0.0958	1.64	0.255	34.4	3.51
	90	0.00	33.88	4.02	24.2	0.1309	0.0923	1.41	0.248	34.4	3.20
	120	0.00	36.61	4.31	26.2	0.1285	0.0906	1.74	0.240	34.3	2.96
	150	0.00	38.11	4.64	27.4	0.1271	0.0896	1.84	N/A	N/A	N/A

minutes follow a similar trend to that observed by Szijártó et al.[36] and Samaniuk et al.,[37] both of whom used rotational rheometers. The in-line technique herein discussed, however, avoided some difficulties associated with rotational rheometers due to its ability to perform measurements on much larger sample sizes. The rheograms represent averaged properties of approximately 8 kg of sample that flow through the magnet during each acquisition; each image acquisition took approximately 1 min. The instrument used in our work also avoided so called "gap size effects," that occur when a rheometer has a gap or channels of a size comparable to the particle size. In this work, the pipe diameter used in our instrument was much larger than the cellulosic particles used.[18]

The time evolution of sugars for each fiber type is shown in Table 2. In Figure 5a, the evolution of glucose concentration is plotted, which was the main sugar produced, and in Figure 5b the conversion is shown. As expected, larger concentrations of glucose were produced with the more concentrated substrate (200EZ, or short fibers, at 16% (w/w) solids). The conversion was calculated using the procedure from Roche et al.[11] as a measure of overall conversion and was similar for both fiber types, approaching 30% after 2 h of hydrolysis. Conversions between 25% and 35% were reported by Um and Hanley[32] (depending on the agitation speed used) during the first 6 h for the hydrolysis of 10% Solka Floc in a baffled reactor with a Rushton impeller using an enzyme loading of 20 filter paper units/g of cellulose. The rate of sugar production in the flow reactor used in our experiment, thus, was similar to those obtained using standard agitated tanks.

To assess changes in fiber shape over time, fiber lengths and widths were measured from the quenched samples taken at different hydrolysis times. In Figures 6a, b, the evolution of length-weighted fiber length and length-weighted fiber width are plotted as a function of conversion. Of these two geometrical parameters, the variable that exhibited the most significant change during hydrolysis was fiber length, whereas fiber width was virtually unchanged over the course of the hydrolysis time studied. The micrographs shown in Figures 2 and 4 confirm that a reduction in fiber length occurred. This suggests a mechanism of particle size reduction where the fiber aspect ratio (a_r = fiber length/fiber width) decreased with the progress of hydrolysis. In other words, the fibers became shorter over time. This behavior can be described through a linear model for length reduction: $L=L_0(1-k_lX)$, where L is the average fiber length, L_0 is the initial average fiber length, X is the conversion, and k_l is a constant, as shown in Figure 6. k_l was 1.44 ± 0.17 and 0.96 ± 0.15 for the long and short fibers, respectively. The width remains constant at its initial value $W \approx W_o$. Therefore, the average aspect ratio a_r evolves as

$$a_r = a_{r0}(1-k_lX), \tag{2}$$

where a_{r0} is the initial aspect ratio. The reduction in length is attributed to the combined action of enzymes and pumping. Prior to addition of the enzymes, our suspensions displayed stable rheological behavior. In previous work, without the addition of enzymes[18] no noticeable changes in rheology over time were observed. In previous work, with addition of enzymes but no pumping,[10] changes in fiber mechanical properties were observed, but they took place over longer timescales than with pumping. These results suggest a combined action of mechanical and enzymatic action in causing the reduction in fiber length.

The results are consistent with reductions in average fiber length during enzymatic hydrolysis reported by Mooney et al.[38] and Ramos et al.[39] and have implications for the modeling of hydrolysis. In a class of mechanistic models of hydrolysis, it is assumed that the cylindrical particles undergo "shrinking" or superficial erosion such that the aspect ratio remains constant[40] or increases,[41] while the number of particles remains constant. Experiments on size distributions during hydrolysis,[38,42] however, indicate significant initial fragmentation of large particles, suggesting a mechanism for initial size reduction where the longer fibers break down into shorter fragments due to loss of mechanical strength caused by enzymatic attack. According to Thygesen et al.,[43] the initial breakdown mechanism consists of fibers being cut into shorter segments between dislocations or slip planes. After the initial fiber shortening, the "shrinking" mechanisms based on surface erosion are expected to become more prevalent. The change in particle shape that

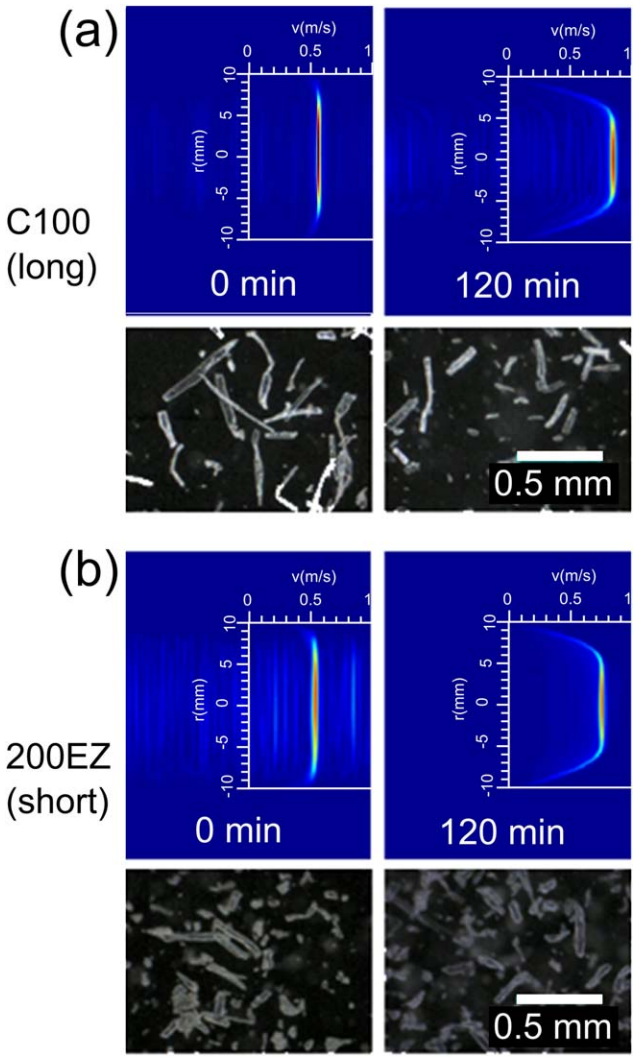

Figure 2. Example velocity images and micrographs obtained at different hydrolysis times for (a) long and (b) short fibers.

The horizontal axis on the velocity profile images represents the velocity and the vertical axis the radial position. [Color figure can be viewed in the online issue, which is available at wileyonlinelibrary.com.]

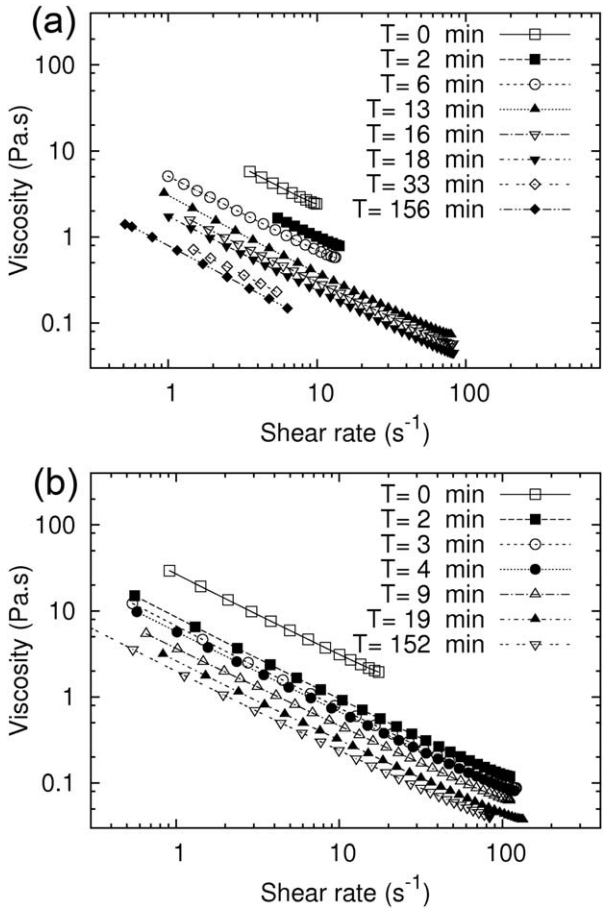

Figure 3. Viscosity as a function of shear rate for various time points during hydrolysis for (a) long fibers and (b) short fibers.

Trends show shear-thinning behavior and a decrease in viscosity with the progress of hydrolysis. All measurements in this figure were made inline using the magnetic resonance-based rheometer.

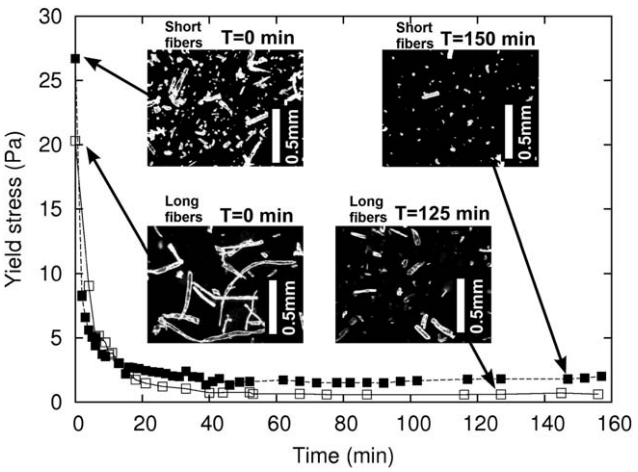

Figure 4. Time-resolved measurements of yield stress during enzymatic hydrolysis.

Micrographs show fiber morphology initially and at a later stage of hydrolysis. Initial length-weighted fiber lengths were 0.444 and 0.331 mm for the long and short fibers, respectively. Final fiber dimensions were 0.272 and 0.240 mm for the long and short fibers, respectively. Fiber dimensions at intermediate times are listed in Table 2.

occurred during initial hydrolysis brings into question whether using solids fraction or volume fraction is sufficient to characterize the tendency to flow of a biomass suspension.

The effect of fiber aspect ratio on rheological properties has been reported previously for pulps.[16] In this context, the changes in rheology are not only due to the decrease in solids concentration but also due to the changes in particle shape. This combined effect of particle concentration and shape explains the extremely rapid decrease in viscosity that can occur during the initial stage of hydrolysis with the value of yield stress being reduced to about 10% of its initial value within 15 min. At conversions lower than 10%, the yield stress had already decreased to a value below 10 Pa, a value that has been used as a criterion for liquefied or "pourable" slurry.[14]

The influence of both particle concentration and aspect ratio on rheology is best illustrated in Figures 7a, b where the yield stresses as a function of the fraction of solids and volume fraction are plotted, respectively. It was observed

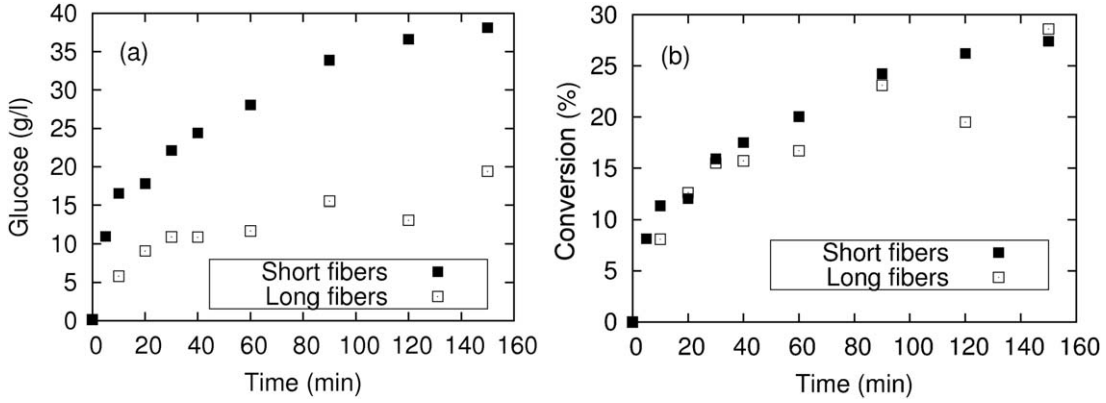

Figure 5. (a) Glucose concentration and (b) conversion[11] as a function of hydrolysis time for both long (□) and short (■) fibers.

that for both fiber types, the yield stress changes rapidly over a small range of concentration. For the longer C100 fibers that had a larger initial aspect ratio, the large change in yield stress occurred at an insoluble solids concentration of around 7% (w/w). In contrast, for the shorter 200EZ fibers, with smaller aspect ratio, the large change in yield stress occurs at a concentration of around 15% (w/w) solids. A similar trend is observed in Figure 7b for the yield stress as a function of solids volume fraction. Because two substrates at significantly different concentrations behave similarly, these measurements clearly show that the slurry rheology depends not only on cellulose concentration, but also on fiber characteristics such as their length-to-diameter ratio. In other words, a slurry of longer fibers can have rheological properties that make pumping difficult at much smaller solids loadings than a slurry of shorter fibers. Such distinction is of particular interest for substrates having particles with large aspect ratios.

Crowding numbers, (N), which represent the combined effect of aspect ratio and volume fraction, were calculated from the measured fiber lengths and widths[17] and from the volume fractions. The volume fraction as a function of the conversion is approximately linear for the initial hours of hydrolysis[11]

$$\phi=\phi_0(1-k_xX), \tag{3}$$

where ϕ is the volume fraction as a function of the conversion, X, and ϕ_0 is the initial volume fraction where k_x is the sum of the initial mass fractions of glucan and xylan (Table 1).

A plot of yield stress as a function of crowding number is shown in Figure 8. It was observed that the yield stress appeared to be a function of the crowding number. For the initial stages of hydrolysis, the yield stress can be estimated by a semilogarithmic function

$$\log \tau_y=a+bN, \tag{4}$$

where a and b are fitting constants, as shown in Figure 8. Substituting expressions for the aspect ratio (Eq. 2) and volume fraction (Eq. 3) as a function of the conversion, one can obtain an estimate of the yield stress as a function of conversion

$$\log \tau_y=a+b\ \ 2/3\phi_0(1-k_xX)[a_{r0}(1-k_lX)]^2, \tag{5}$$

The equation shows that the relationship between yield stress and conversion is highly nonlinear and depends strongly on fiber shape properties such as the initial aspect ratio.

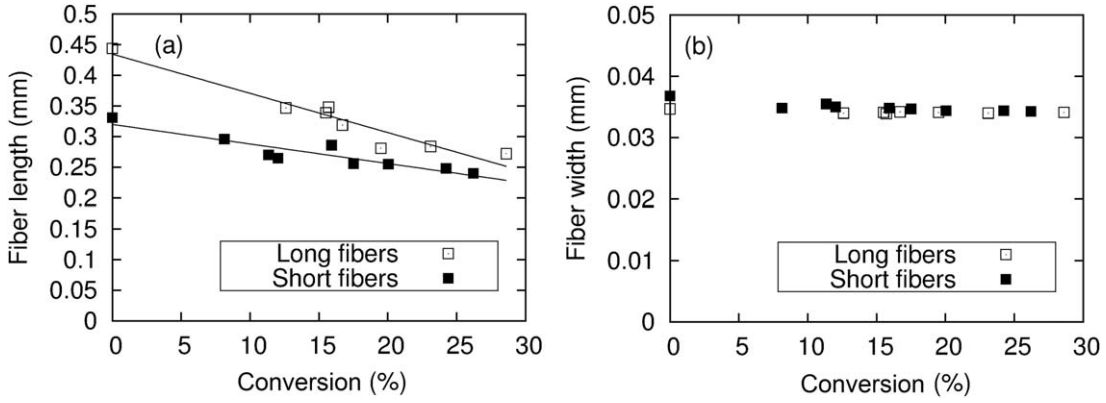

Figure 6. (a) Fiber length-weighted length and (b) fiber length-weighted width as a function of the conversions of the cellulosic fibers.

Linear trends of fiber length as a function of conversion given by $L=L_0(1-k_lX)$ are shown in (a), whereas fiber width remains constant for both fibers as a function of conversion, as shown in (b). In (a), k_l is 1.44 ± 0.17 and 0.96 ± 0.15 for the long and short fibers, respectively.

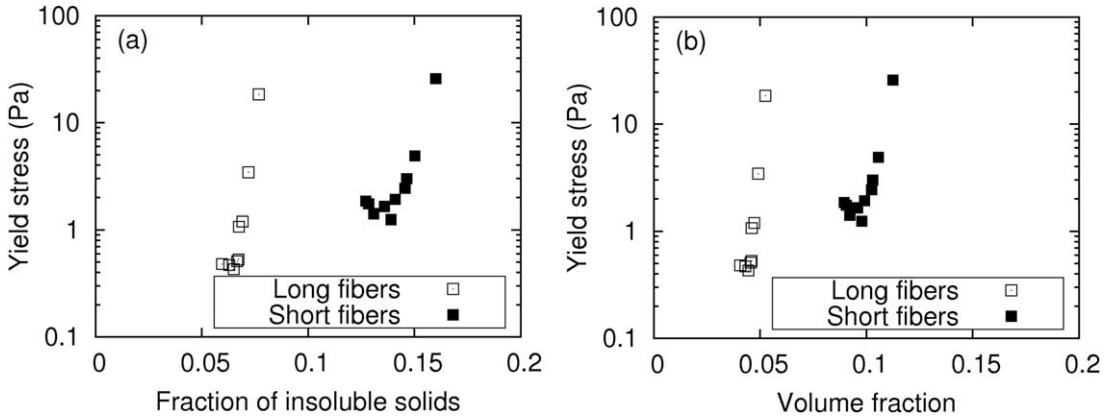

Figure 7. (a) Yield stress as a function of insoluble solids, and (b) yield stress as a function of fiber volume fraction.

In Figure 9, we plot the crowding number as a function of time. The trend is similar to that observed for the yield stress, namely a rapid decrease occurs initially for both fiber types and a steady value is reached afterward. It is clear from our results that the concept of crowding number is expected to be most useful for substrates that contain a significant amount of long fibers ($a_r \gg 1$), whereas for near spherical particles, N becomes approximately equal to the volume fraction multiplied by a constant of proportionality. In such case, the volume fraction is expected to be an adequate variable for correlating concentration and rheology.

It should be noted that the focus of the present model is on the early stages of hydrolysis, when aspect ratios are larger, volume fractions as a function of conversion are linear and conventional kinetic models fail to predict hydrolysis kinetics.[11,15]

As defined in this work, the crowding number requires measurement of fiber lengths, which requires specialized instrumentation. In the absence of fiber length measurements, fiber aspect ratios could be indirectly described through variables, such as the maximum packing fraction (volume fraction of a settled bed of fibers). It must also be noted that in this work the fibers used had similar composition, but this may not be the case in general, and the rheology is expected to be influenced by fiber properties other than fiber aspect ratio and volume fraction. Characteristics such as fiber stiffness, amount of dislocations, and surface interactions would vary upon substrate and pretreatment used and may have different effects on the rheology of biomass suspensions.

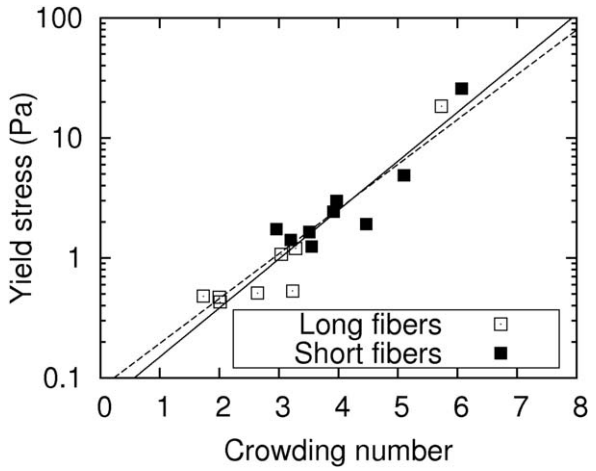

Figure 8. Yield stress as a function of the crowding number for both long (□) and short (■) fibers. Also shown are the linear fits obtained as given in Eq. 4, with the one for the longer fibers given as a solid line, and the one for the shorter fibers given as a dashed line.

a is -1.23 ± 0.19 for the longer fibers and -1.1 ± 0.3 for the shorter fibers, and b is 0.41 ± 0.06 for the longer fibers and 0.37 ± 0.07 for the shorter fibers, for yield stress in Pascals.

Conclusions

Suspensions of two types of cellulosic fibers differing in fiber aspect ratio were hydrolyzed in a 10-L recycle reactor with on-line rheological measurements performed using MRI. Hydrolysis rates in the recycle reactor configuration were comparable to rates previously reported for stirred tanks. The MRI rheometry method permitted the acquisition and calculation of rheograms and yield stress values at rates of up to one per minute. It was observed that a large decrease in yield stress occurred during the initial stages, decreasing to below 10 Pa during the first 5 min of hydrolysis. The rapid rheological changes took place when fibers

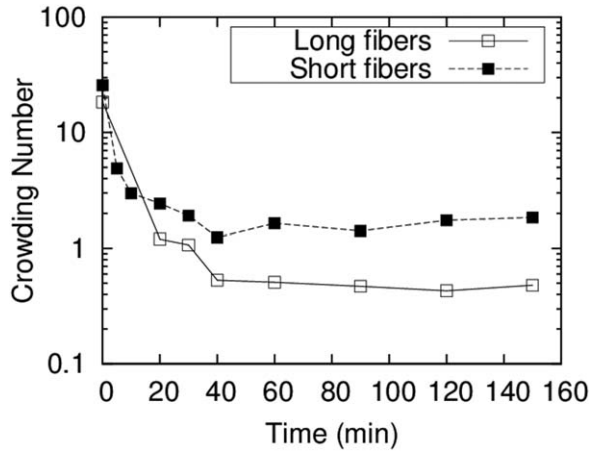

Figure 9. Crowding number as a function of time for both long (□) and short (■) fibers.

Both fibers start at approximately the same crowding number and follow similar trends to those observed in changes in yield stress (Figure. 4).

underwent less than 10% conversion. Yield stress changes occurred within a narrow range of mass fractions that were very different for each fiber type. This was attributed to the differences in initial fiber length among the two fiber types. Measurements of fiber length and width changes during hydrolysis revealed that length was the dimension that underwent the most rapid changes. This suggests a hydrolysis mechanism initially dominated by fragmentation by which fiber aspect ratio decreases as conversion progresses. The influence of particle length and concentration on rheology helps to explain the differences reported with biomass having particles with different aspect ratios. A simple model was proposed that describes the effects of fiber concentration and aspect ratio on the yield stress. Materials with long and thin fibers, such as softwoods, display rheological challenges at lower concentrations than substrates with lower aspect ratio particles, such as pretreated corn stover. Conditions that present rheological challenges, therefore, cannot be predicted solely by solid content or volume fraction, but will depend also on particle shape. In this work, crowding numbers were a useful indicator of the degree of interfiber interactions that influence the rheology of cellulosic suspensions undergoing hydrolysis. Use of this variable is expected to facilitate process optimization via hydrolysis models in which rheological properties and reaction kinetics are linked.

Acknowledgments

The authors would like to thank Tom Lindström of Innventia AB in Stockholm, Sweden, for performing the fiber size measurements. The magnetic resonance imaging pulse sequences used in this study were provided by Aspect Imaging, Hevel Modi'in Industrial Area, Israel. Partial financial support was provided by the Center for Process Analytical Chemistry at the University of Washington, Seattle, WA. The authors declare that they have no conflicts of interest related to the publication of this work.

Notation

a = fitting parameter for yield stress as a function of crowding number
b = fitting parameter for yield stress as a function of crowding number
a_r = fiber aspect ratio
a_{r0} = initial fiber aspect ratio
FIS = fraction of insoluble solids
k_l = fitting parameter for fiber length as a function of conversion
k_x = fitting parameter for volume fraction as a function of conversion
L = length-weighted fiber length, mm
L_0 = initial length-weighted fiber length, mm
L_P = pipe length, m
N = crowding number
r = radial position within pipe, cm
v = velocity, cm/s
W = length-weighted fiber width, μm
W_0 = initial length-weighted fiber width, μm
X = conversion
$\dot{\gamma}$ = shear rate, s^{-1}
ΔP = pressure drop in pipe, Pa
τ_y = yield stress, Pa
ϕ = fiber volume fraction
ϕ_0 = initial fiber volume fraction

Literature Cited

1. Banholzer WF, Watson KJ, Jones ME. How might biofuels impact the chemical industry? *Chem Eng Prog*. 2008;104:C7–C14.
2. Galbe M, Sassner P, Wingren A, Zacchi G. Process engineering economics of bioethanol production. *Adv Biochem Eng Biotechnol*. 2007;108:303–327.
3. Hoyer K, Galbe M, Zacchi G. Production of fuel ethanol from softwood by simultaneous saccharification and fermentation at high dry matter content. *J Chem Technol Biotechnol*. 2009;84:570–577.
4. Humbird D, Mohagheghi A, Dowe N, Schell DJ. Economic impact of total solids loading on enzymatic hydrolysis of dilute acid pretreated corn stover. *Biotechnol Prog*. 2010;26:1245–1251.
5. Jørgensen H, Vibe-Pedersen J, Larsen J, Felby C. Liquefaction of lignocellulose at high-solids concentrations. *Biotechnol Bioeng*. 2007;96:862–870.
6. Sassner P, Galbe M, Zacchi G. Techno-economic evaluation of bioethanol production from three different lignocellulosic materials. *Biomass Bioenergy*. 2008;32:422–430.
7. Vane LM. Separation technologies for the recovery and dehydration of alcohols from fermentation broths. *Biofuels Bioprod Biorefin*. 2008;2:553–588.
8. Varga E, Klinke HB, Réczey K, Thomsen AB. High solid simultaneous saccharification and fermentation of wet oxidized corn stover to ethanol. *Biotechnol Bioeng*. 2004;88:567–574.
9. Xue Y, Jameel H, Phillips R, Chang H-M. Split addition of enzymes in enzymatic hydrolysis at high solids concentration to increase sugar concentration for bioethanol production. *J Ind Eng Chem*. 2012;18:707–714.
10. Lavenson DM, Tozzi EJ, Karuna N, Jeoh T, Powell RL, McCarthy MJ. The effect of mixing on the liquefaction and saccharification of cellulosic fibers. *Bioresour Technol*. 2012;111:240–247.
11. Roche CM, Dibble CJ, Knutsen JS, Stickel JJ, Liberatore MW. Particle concentration and yield stress of biomass slurries during enzymatic hydrolysis at high-solids loadings. *Biotechnol Bioeng*. 2009; 104:290–300.
12. Bennington C, Kerekes R, Grace J. The yield stress of fibre suspensions. *Can J Chem Eng*. 1990;68:748–757.
13. Knutsen JS, Liberatore MW. Rheology of high-solids biomass slurries for biorefinery applications. *J Rheol*. 2009;53:877–892.
14. Stickel JJ, Knutsen JS, Liberatore MW, Luu W, Bousfield DW, Klingenberg DJ, Scott CT, Root TW, Ehrhardt MR, Monz TO. Rheology measurements of a biomass slurry: an interlaboratory study. *Rheol Acta*. 2009;48:1005–1015.
15. Zhang J, Shao X, Lynd LR. Simultaneous saccharification and cofermentation of paper sludge to ethanol by Saccharomyces cerevisiae RWB222. Part II: investigation of discrepancies between predicted and observed performance at high solids concentration. *Biotechnol Bioeng*. 2009;104:932–938.
16. Dalpke B, Kerekes R. The influence of fibre properties on the apparent yield stress of flocculated pulp suspensions. *J Pulp Pap Sci*. 2005;31:39–43.
17. Kerekes R, Schell C. Characterization of fibre flocculation regimes by a crowding factor. *J Pulp Pap Sci*. 1992;18:J32–J38.
18. Lavenson DM, Tozzi EJ, McCarthy MJ, Powell RL. Yield stress of pretreated corn stover suspensions using magnetic resonance imaging. *Biotechnol Bioeng*. 2011;108:2312–2319.
19. Arola DF, Barrall GA, Powell RL, McCarthy KL, McCarthy MJ. Use of nuclear magnetic resonance imaging as a viscometer for process monitoring. *Chem Eng Sci*. 1997;52:2049–2057.
20. McCarthy K, Kauten R, McCarthy M, Steffe J. Flow profiles in a tube rheometer using magnetic resonance imaging. *J Food Eng*. 1992;16:109–125.
21. Pimenova NV, Hanley TR. Effect of corn stover concentration on rheological characteristics. *Appl Biochem Biotechnol*. 2004;114:347–360.
22. Tozzi EJ, Bacca LA, Hartt WH, McCarthy KL, McCarthy MJ. Robust processing of capillary velocimetry data via stress-rescaled velocity functions. *J Rheol*. 2012;56:1449–1464.
23. Hames B, Ruiz R, Scarlata C, Sluiter A, Sluiter J, Templeton D. Preparation of samples for compositional analysis. Laboratory Analytical Procedure, National Renewable Energy Laboratory, Golden, CO, NREL/TP-510–42620.2005.
24. Sluiter A, Hames B, Ruiz R, Scarlata C, Sluiter J, Templeton D. Determination of ash in biomass. Laboratory Analytical Procedure, National Renewable Energy Laboratory, Golden, CO, NREL/TP-510–42620. 2008.
25. Sluiter A, Hames B, Ruiz R, Scarlata C, Sluiter J, Templeton D, Crocker D. Determination of structural carbohydrates and lignin in biomass. Laboratory Analytical Procedure, National Renewable Energy Laboratory, Golden, CO, NREL/TP-510–42618. 2008.

26. Dowe N, McMillan J. SSF Experimental Protocols—Lignocellulosic Biomass Hydrolysis and Fermentation. Laboratory Analytical Procedure, National Renewable Energy Laboratory, Golden, CO, NREL/TP-510–42630.2008.
27. Pulkkinen I, Ala-Kaila K, Aittamaa J. Characterization of wood fibers using fiber property distributions. *Chem Eng Process. Process Intensif.* 2006;45:546–554.
28. Li B, Bandekar R, Zha Q, Alsaggaf A, Ni Y. Fiber quality analysis: optest fiber quality analyzer vs. L & W fiber tester. *Ind Eng Chem Res.* 2011;50:12572–12578.
29. Dunaway KW, Dasari RK, Bennett NG, Eric Berson R. Characterization of changes in viscosity and insoluble solids content during enzymatic saccharification of pretreated corn stover slurries. *Bioresour Technol.* 2010;101:3575–3582.
30. Ehrhardt M, Monz T, Root T, Connelly R, Scott C, Klingenberg D. Rheology of dilute acid hydrolyzed corn stover at high solids concentration. *Appl Biochem Biotechnol.* 2010;160:1102–1115.
31. Rosgaard L, Andric P, Dam-Johansen K, Pedersen S, Meyer AS. Effects of substrate loading on enzymatic hydrolysis and viscosity of pretreated barley straw. *Appl Biochem Biotechnol.* 2007;143:27–40.
32. Um BH, Hanley TR. High-solid enzymatic hydrolysis and fermentation of solka floc into ethanol. *J Microbiol Biotechnol.* 2008;18:1257–1265.
33. Viamajala S, McMillan JD, Schell DJ, Elander RT. Rheology of corn stover slurries at high solids concentrations–effects of saccharification and particle size. *Bioresour Technol.* 2009;100:925–934.
34. Wiman M, Palmqvist B, Tornberg E, Lidén G. Rheological characterization of dilute acid pretreated softwood. *Biotechnol Bioeng.* 2011;108:1031–1041.
35. Pimenova N, Hanley T. Measurement of rheological properties of corn stover suspensions. *Appl Biochem Biotechnol.* 2003;105:383–392.
36. Szijártó N, Siika-Aho M, Sontag-Strohm T, Viikari L. Liquefaction of hydrothermally pretreated wheat straw at high-solids content by purified Trichoderma enzymes. *Bioresour Technol.* 2011;102:1968–1974.
37. Samaniuk JR, Tim Scott C, Root TW, Klingenberg DJ. The effect of high intensity mixing on the enzymatic hydrolysis of concentrated cellulose fiber suspensions. *Bioresour Technol.* 2011;102:4489–4494.
38. Mooney CA, Mansfield SD, Beatson RP, Saddler JN. The effect of fiber characteristics on hydrolysis and cellulase accessibility to softwood substrates. *Enzyme Microbial Technol.* 1999;25:644–650.
39. Ramos L, Nazhad M, Saddler J. Effect of enzymatic hydrolysis on the morphology and fine structure of pretreated cellulosic residues. *Enzyme Microbial Technol.* 1993;15:821–831.
40. Movagharnejad K, Sohrabi M. A model for the rate of enzymatic hydrolysis of some cellulosic waste materials in heterogeneous solid–liquid systems. *Biochem Eng J.* 2003;14:1–8.
41. Griggs AJ, Stickel JJ, Lischeske JJ. A mechanistic model for enzymatic saccharification of cellulose using continuous distribution kinetics I: depolymerization by EGI and CBHI. *Biotechnol Bioeng.* 2012;109:665–675.
42. King K. Enzymic degradation of crystalline hydrocellulose. *Biochem Biophys Res Commun.* 1966;24:295–298.
43. Thygesen LG, Hidayat BJ, Johansen KS, Felby C. Role of supramolecular cellulose structures in enzymatic hydrolysis of plant cell walls. *J Ind Microbiol Biotechnol.* 2011;38:975–983.

Manuscript received Nov. 19, 2013, and revision received Dec. 31, 2013.